HOSTED BY
ELSEVIER
Available online at www.sciencedirect.com
ScienceDirect
Soils and Foundations 61 (2021) 1419–1430
www.elsevier.com/locate/sandf

Technical Paper

Failure envelopes of pile groups under combined axial-moment loading: Theoretical background and experimental evidence

L. de Sanctis [a], R. Di Laora [b,*], R.M.S. Maiorano [a], G. Favata [c], S. Aversa [a]

[a] University of Naples Parthenope, Naples, Italy
[b] University of Campania Luigi Vanvitelli, Aversa (CE), Italy
[c] Enel Green Power, Roma, Italy

Received 19 March 2021; received in revised form 19 July 2021; accepted 14 August 2021
Available online 3 September 2021

Abstract

The problem of failure envelopes of pile groups subjected to vertical and eccentric load is investigated both theoretically and experimentally. A critical review of literature works on failure envelopes for pile groups under combined axial-moment loading is first provided. Emphasis is placed on a recent, exact solution derived from theorems of limit analysis by idealizing piles as uniaxial rigid-perfectly plastic elements. The application of the relevant equations over a practical range of problems needs only the axial capacities in compression and uplift of the isolated piles. An intense program of centrifuge experiments carried out along with different load paths on annular shaped pile groups aimed at validating the equations pertinent to the above solution is presented and discussed. The end-points of the load paths followed in the centrifuge lie approximately above the analytical failure envelope, giving confidence that the reference equations can be reliably adopted to assess the capacity of a pile group under combined axial-moment loading. Finally, the kinematics of the collapse mechanism observed experimentally is compared to that determined from the application of the reference theory.

Keywords: Centrifuge modelling; Pile group; Eccentric loading; Failure envelopes

1. Introduction

Innovative foundation solutions are being contemplated in recent time to accommodate the large demand from energy and communication industry of tall structures subjected to cyclic, multi-component loads. However, recent theoretical research works indicate that current industry-based methodologies often lead to overconservative – and thereby uneconomic – design. Tall wind turbines are a paradigmatic example in this sense. In this situation, the load transmitted by the tower under extreme wind conditions is extremely eccentric and the shallow foundation, with its dead load, has to reduce the eccentricity within reasonable limits, with the primary aim of avoiding a bearing capacity failure or the overturning of the whole structure. The need of matching the above limit may lead to foundation mats with very large diameters. In this circumstance, a piled foundation is the first alternative, at least in the onshore environment. The horizontal load is a small percentage of the axial load, so as, from an engineering standpoint, this problem can be conveniently idealized as a foundation subjected to purely vertical, eccentric load. For instance, Iovino et al. (2021) have documented the case study of a wind farm south to Italy with 95 m high wind turbines, for which the horizontal load under extreme wind conditions is only 5% the dead load of the structure, includ-

Peer review under responsibility of The Japanese Geotechnical Society.
* Corresponding author at: Department of Engineering, University of Campania Luigi Vanvitelli, Aversa, Italy.

https://doi.org/10.1016/j.sandf.2021.08.002
0038-0806/

ing the weight of the foundation cap. In this situation, the most widespread approach is to identify the ultimate limit state of the whole foundation with the mobilization of the axial capacity on the outermost pile. Such an approach, recommended for example by AASHTO Bridge Design Specification (2012), is unduly conservative. In fact, the attainment of the axial capacity on the outermost pile does not represent a failure condition but merely the onset of yielding. At this point, the foundation is still capable to carry out a further increment of the external load taking advantage form the ductility of the soil-foundation system, i.e. there is still room for individual piles belonging to the group to progressively achieve their axial capacity in compression or uplift.

The excess of conservatism coming from the above approach is recognized by some codes and provisions. The Eurocode 7 (CENT/TC 250, 2003), as an example, recommends that 'for piles supporting a stiff structure, a failure will occur only if a significant number of piles fails together', meaning that 'a failure mode involving only one pile need not be considered'. An alternative approach, referred to as 'fully plastic calculation', can be found in FEMA 750 (2009). However, the same recommended provisions advertise that 'the plastic analysis approach is likely to overestimate the strength that a multi-pile group is capable of developing', outlining that 'many engineers would prefer the conventional approach'. Overall, while codes seem aware of the inherent conservatism of the conventional method, they do not provide any guideline on how to evaluate the increase of strength that a pile group may provide after the outermost pile has achieved its axial capacity. In the authors' opinion, this situation can be attributed to the limited attention that the problem of failure envelopes of piled foundations has received in literature.

The concept of failure envelopes has been applied extensively in the last decades to many foundation types, including surface foundations (Nova & Montrasio 1991, Butterfield and Gottardi 1994, Taiebat & Carter 2000, Gourvenec & Randolph 2003, Gourvenec 2007, Vulpe et al. 2014), skirted and caisson foundations (Bransby & Randolph 1998, Gourvenec & Barnett 2011) and spudcan foundations (Martin and Houlsby, 2001, Cassidy et al., 2004). The advantage of this approach over classical superposition (Brinch Hansen, 1970) is manifold as widely discussed in Nova & Montrasio (1991) and Gottardi & Butterfield (1993). Failure envelopes can be used to assess the capacity and proximity to failure surface under combined loading or to develop plasticity-based macroelement models. On the other hand, there is limited published work addressing the problem of failure envelopes for piled foundations. In this paper, a review of the literature on this critical issue is first provided. Particularly, the attention is focused on a recent, exact solution derived from theorems of limit analysis (Di Laora et al. 2019). While the advantage of this approach over the assumption of a linear relationship between axial and moment capacities is evident and widely discussed in Di Laora et al. (2019), the validity of the pertinent equations has not yet proven experimentally. To fill this gap, a series of centrifuge tests on annular shaped pile groups has been carried out at the Schofield Center of the University of Cambridge. Details about models preparation, monitoring equipment and testing procedure have been discussed in de Sanctis et al. (2021) As a follow up, this work focuses on the experimental validation of the theoretical framework of Di Laora et al. (2019), the effect of pile variability on the moment capacity of pile groups and the kinematics of the collapse mechanism of pile groups under vertical and eccentric load. Notably, the approach which is being validated is applicable when the resultant action, even if remarkably eccentric, is almost vertical. Of course, there might be circumstances where the inclination of this action is not negligible, as in case of quay walls or squatty bridge piers. In this case, the horizontal component must be properly considered to evaluate the ultimate conditions of the pile group.

2. Failure envelopes of pile groups under vertical eccentric load: A critical review

The problem of the failure envelope of a piled foundation in the (Q, M) plane (Q = axial load, M = moment) has been traditionally investigated on an experimental basis. Such works include experiments on small groups of aluminium piles at reduces scale embedded in both sand (Kishida & Meyerhof 1965, Meyerhof & Ranjan 1973, Meyerhof et al. 1983) and saturated clay (Saffery & Tate 1961, Meyerhof 1981, Meyerhof & Yalcin 1984). As a result of this experimental work, semi-empirical approximate expressions for failure envelopes of pile groups are available. The application in practice of these equations is not immediate because of the inherent difficulties in the evaluation of the relevant parameters, as widely discussed by Di Laora et al. (2019). Moreover, the foregoing tests have concentrated on reduced scale models of small groups in homogeneous soils. Recent research works have also focused on the bearing behaviour of pile groups subjected to inclined and/or eccentric loads by means of numerical analyses (e.g. Papadopoulou & Comodromos 2010, Comodromos & Papadopoulou 2012, Rose et al. 2013, Sheil & McCabe 2014, Franza & Sheil 2021). It is argued from these works that the axial load carried out by a pile group at a prescribed level of vertical displacement decreases with the load eccentricity. However, there are neither ready-to-use equations nor charts from these papers for a practical evaluation of the ultimate limit conditions of a pile group.

A novel, exact solution for failure envelopes of piled foundations in the (Q, M) plane has been determined by Di Laora et al. (2019) throughout the application of the theorems of limit analysis. The assumptions used to derive the pertinent equations are: (a) piles behaving as uniaxial rigid-perfectly plastic elements; (b) the piles' connecting

cap is a rigid body; (c) the connections of the piles to the cap are idealized as hinges, and hence the heads of the piles cannot be subjected to bending moments. This solution allows to define the failure envelope of a pile group in the general case of unevenly distributed, dissimilar piles. The only ingredients needed are the axial capacity in compression, N_u, and in uplift, ($-S_u$), of all piles belonging to the group. The failure envelope is a polygon with $2p$ vertices, whose coordinates are (i, $k = 1, \ldots, p$):

$$\begin{cases} Q_{ui} = \sum_{j=1}^{i-1} N_{uj} - \sum_{j=i}^{p} S_{uj} \\ M_{ui} = -\sum_{j=1}^{i-1} N_{uj} x_j + \sum_{j=i}^{p} S_{uj} x_j \end{cases} \quad i = 1, \ldots, p \tag{1}$$

$$\begin{cases} Q_{uk} = -\sum_{j=1}^{k-1} S_{uj} + \sum_{j=k}^{p} N_{uj} \\ M_{uk} = \sum_{j=1}^{k-1} S_{uj} x_j - \sum_{j=k}^{p} N_{uj} x_j \end{cases} \quad k = 1, \ldots, p \tag{2}$$

where p is the number of piles while x_j is the abscissa of j-th pile along the direction perpendicular to the resultant moment vector. Fig. 1 shows the interaction diagram of a row of 4 equally spaced, identical piles with $S_u = 3/4N_u$. In the realm of the upper bound theorems, the vertices of the interaction diagram correspond to failure modes where the piles' connecting cap displaces by rotation about a point in between two adjacent piles, while the conjunction lines are representative of failure modes where the cap displaces by rotation about the head of a pile. As vertices are singularities, a load path will never end on them in practice. Therefore, a corollary of the foregoing hypotheses is that a pile group cannot but fail by rotating about the head of a pile [a piles' alignment]. In this last mode, all piles achieve their axial capacity in compression or uplift, with the exception of the pile [the piles' alignment] corresponding to the centre [the axis] of rotation. Further developments, including the case of piles' connections to the raft modelled as rigid-plastic fixities can be found in the original paper. The advantage of the proposed solution over the traditional approach is manifold, as demonstrated also by means of an example application to a wind farm south to Italy. Nevertheless, Eqs. (1–2) have never been proven experimentally.

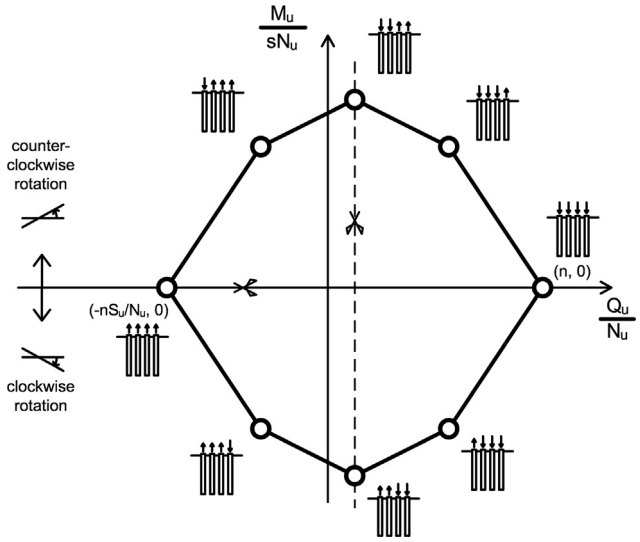

Fig. 1. Failure envelope of a row of four piles (from Di Laora et al. 2019).

3. Evidence from centrifuge experiments

Two series of centrifuge tests were carried out at the Schofield Centre of the University of Cambridge. For the convenience of the reader, a brief description of the experimental set-up and the procedure followed for data processing and representation already discussed in de Sanctis et al. (2021) is offered. Further details on the time-histories of the monitoring data can be found in the original publication.

3.1. Model foundations, soil properties and testing procedure

The two sets of tests were performed at an increased gravity of 50 g on annular shaped groups of 8 piles and isolated piles embedded in kaolin clay. Fig. 2 illustrates the arrangement of the model foundations in the 850 mm diameter cylindrical container adopted for the purpose of the experimental study. The first set of experiments, referred to as set A, included a pile group under centred load, a pile group under highly eccentric load, and two isolated piles, one in compression and one in uplift. The second set, referred to as B, included a pile group under moderately eccentric, compression load, a pile group under moderately eccentric, tension load, and two isolated piles, one in compression and one in uplift.

All the piles were aluminium closed-ended hollow cylinders, 1 mm thick, with an outer diameter of 10 mm (0.5 m at prototype scale) and an overall length of 280 mm (14 m). As shown in the schematic cross section of Fig. 3, they were embedded in the kaolin layer for 240 mm (12 m), with the exception of the isolated piles tested in uplift, whose embedded length is 250 mm (12.5 m). Piles within a group were connected by spherical hinges to an aluminium circular raft with a diameter of 138 mm (6.9 m) and an height of 15 mm (0.75 m), which was clear of the soil. A skirted shape was adopted for each raft so as to minimize the axial load on piles before the execution of the test. The model foundations tested under eccentric load were also equipped with a cantilever beam for the application of the external load.

The clay layer was a slurry prepared by mixing Speswhite clay powder and de-aired water at nearly twice its liquid limit. This type of kaolin has been adopted in many other experimental works at the Schofield Centre, so as its properties are well known (see Table 1). The clay layer was consolidated at 1 g by applying a combination of total vertical stress of 70 kPa at the top and a negative pore pressure of −70 kPa at the base through a vacuum pump. After removing the cylindrical container from the hydraulic press and the connection to the vacuum pump, the vertical total stresses drop to zero (the small 1 g geostatic value may be

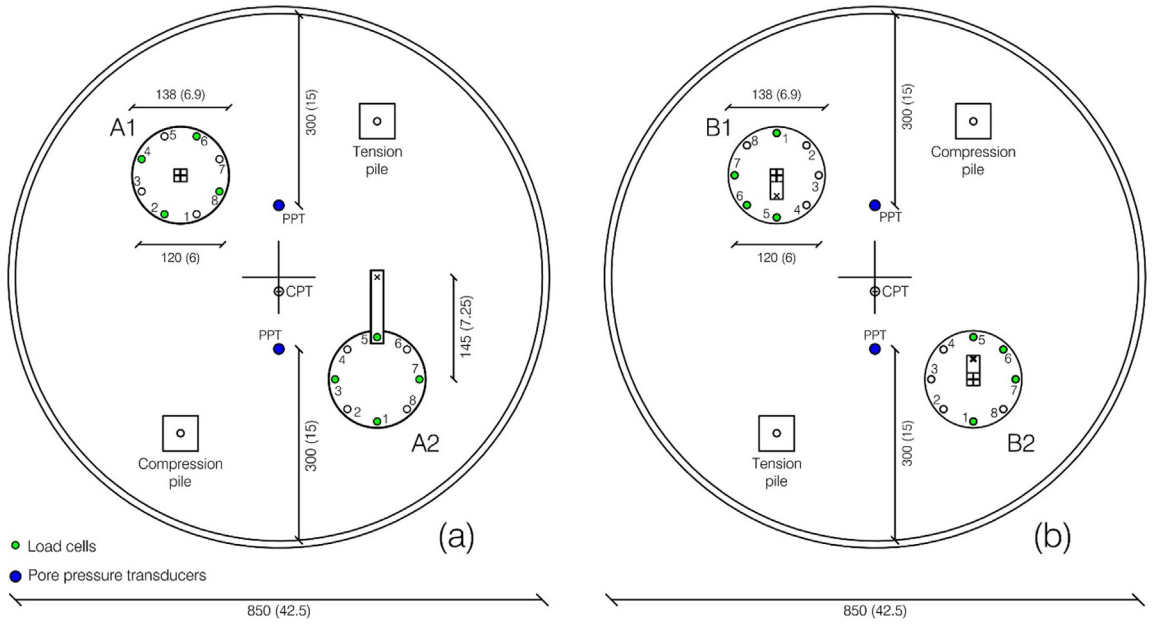

Fig. 2. Layout of model foundations in experiment sets A and B; dimensions (mm) are given at model scale, while dimensions in brackets (m) refer to prototype scale.

disregarded) while the vertical effective stress distribution remains unchanged. At this stage the excess pore pressures are opposite to the vertical effective stresses. The time elapsing from the end of the consolidation stage and the application of the centrifugal acceleration is very short and can be disregarded, so as the vertical effective stress profile after 1 g consolidation can be taken also as the initial profile before the application of the acceleration field in the centrifuge. Aluminium piles were coated with Houston sand ($D_{50} = 0.356$ mm), to simulate the contact of cast-in-situ reinforced concrete piles and were installed by pushing them into the clay layer at 1 g. Installation generated a change of effective stress tensor and positive excess pore pressure locally around the pile, which are difficult to evaluate. However, the scope of this work is not to investigate installation effects, but rather to compare the combined axial-moment capacity of the groups with the failure envelopes determined from (S_u, N_u). This is a consistent comparison in that the disturbance caused by installation is the same for isolated piles and piles belonging to the groups.

The model foundations were equipped with (a) vertically mounted Linear Variable Differential Transformers (LVDTs), to measure their settlements; (b) Micro-Electro-Mechanical-Systems (MEMS) accelerometers, for monitoring their rotations; (c) miniaturised Load Cells (LCs), to measure axial loads on piles; (d) Pore water Pressure Transducers (PPTs), for recording pore water pressures within the soil mass. The layout of all the miniaturised devices is shown in Figs. 3 and 4. Load cells were positioned immediately beneath the spherical hinges. For each raft, only half of the piles were equipped with LCs. For set A, the external load transmitted by the actuator was evaluated from the axial loads recorded by the load cells installed at the top of the piles. For set B, the driving actuator was also equipped with a load cell, and a direct measurement of the external load on the pile groups was also available. Spherical hinges allow a direct and straightforward interpretation of the load distribution among piles, provided that the external moment cannot be but equilibrated by axial loads on piles. Only one LVDT was mounted on each raft. As each circular raft adopted in the experiments behaves like a rigid body, the displacement of any pile can be evaluated by combining the recordings from the LVDT and the MEMS accelerometers.

Fig. 5 shows are the profiles of undrained shear strength c_u obtained from two Cone Penetration Tests (CPTs) carried out with a miniaturised device, with a diameter of 6.35 mm and 60-degree cone tip. Notably, while CPT No. 1 (set A) was carried out at 1 g after the swing down stage, CPT No. 2 (Set B) was performed in flight after re-consolidation of the clay. The theoretical profile of c_u determined from the Critical State Soil Mechanics theory (Roscoe et al. 1958) with soil parameters summarized in Table 1 and the effective vertical stress corresponding to U = 70 % is in a very satisfactory agreement with that obtained from the CPT No. 2. The above theoretical solution was therefore taken as the reference profile for the experiments under examination.

A crucial point of the experimental procedure is the application of the load history. In all cases, the external load was applied under displacement control, by setting the displacement rate of the driving actuator at 1 mm/s. The external load was applied on the end of the cantilever beam attached to the cap, through a miniaturised spherical ball, so that it could be idealized as a point load. The load

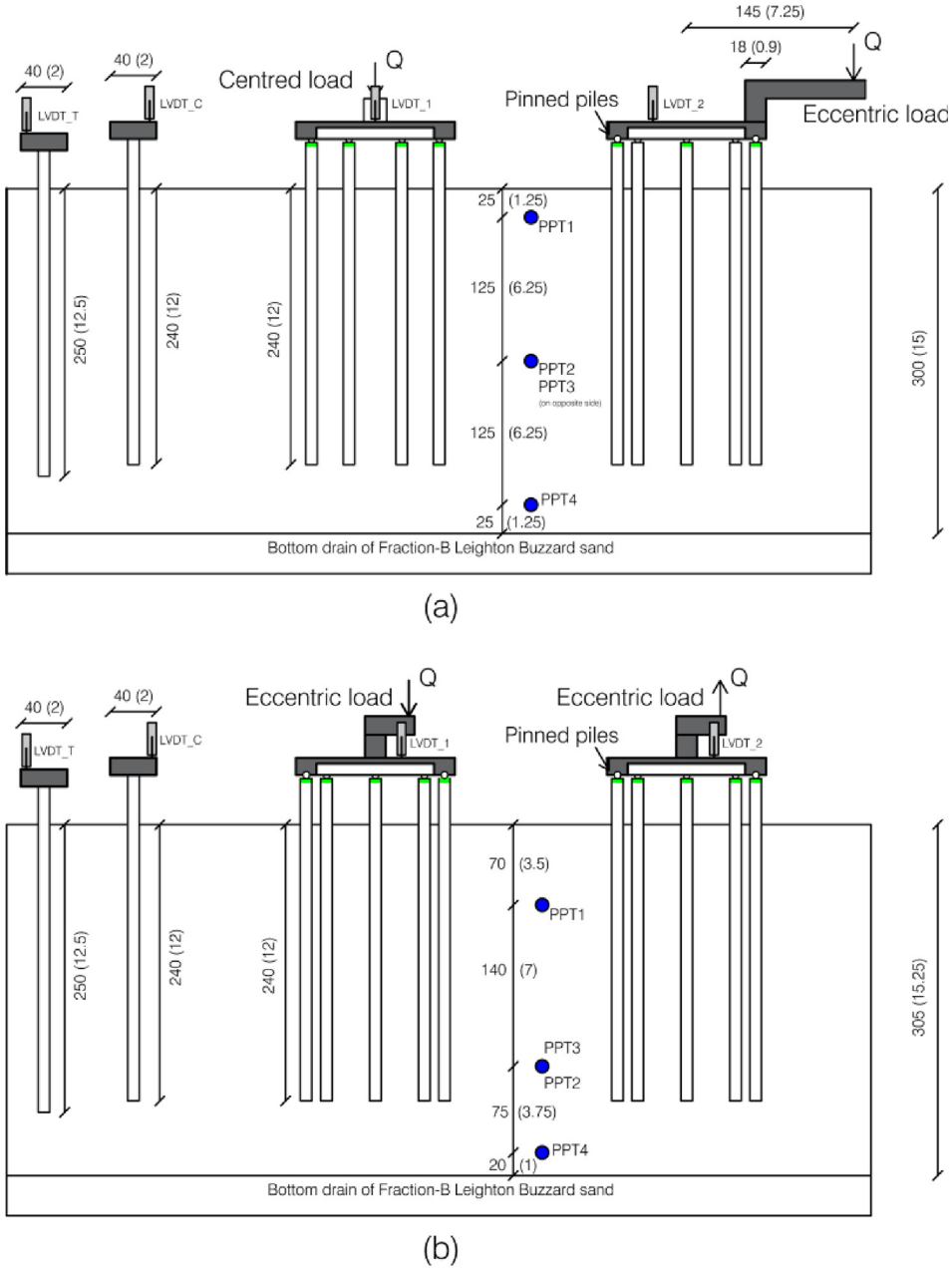

Fig. 3. Schematic cross sections of foundation models for sets A and B, dimensions (mm) are given at model scale, while dimensions in brackets (m) refer to prototype scale.

on pile groups was applied under constant eccentricity and, hence, the direction of the load path in the (Q, M) plane is known a-priori; this allowed an easy identification of the moment load corresponding to the collapse of the group.

3.2. Axial-moment capacity of the foundation models

The axial capacities evaluated from loading tests on isolated piles for Sets A and B are summarised in Table 2. They have been calculated using the following relationship:

$$N_u[-S_u] = Q_{\max}[Q_{\min}] + W \quad (3)$$

where $Q_{\max}$ [$Q_{\min}$] is the maximum [minimum] value of the recorded load and W the weight of the capped pile.

Table 1
Properties of speswhite kaolin clay.

Plastic limit PL (%)	30
Liquid limit LL (%)	63
Plasticity Index PI (%)	33
Specific gravity Gs	2.6
Slope of critical state line (CSL) in q-p plane, M	0.9
Slope of unloading–reloading line, κ	0.039
Intercept of CSL at p' = 1 kPa, Γ	3.31
Slope of normal consolidation line, λ	0.22

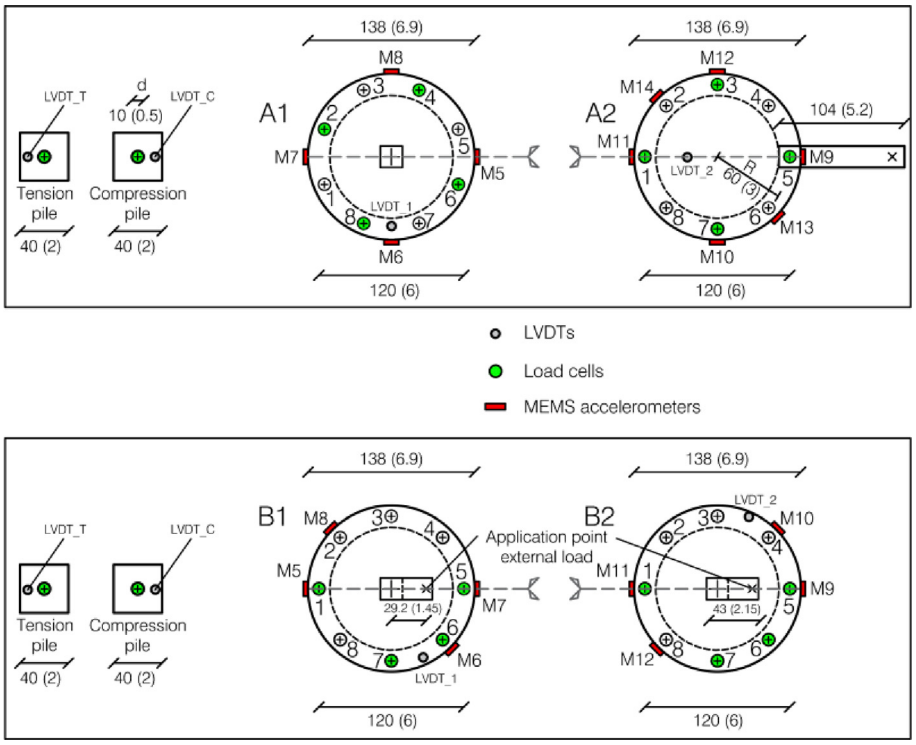

Fig. 4. Plan view of monitoring devices mounted on model foundations; dimensions (mm) are given at model scale, while dimensions in brackets (m) refer to prototype scale.

Fig. 6 illustrate the load settlement response of pile group A1, subjected to centred load, and the load rotation curve evaluated for pile group A2, subjected to eccentric load. For this last curve, the applied external load Q is plotted against the quantity (θśR), with R being the radius of the circle passing through the piles, in order to allow a comparison with the settlement needed to mobilize the capacity of pile group A1. For both the examined models, the driving actuator was not equipped with a load cell and, therefore, the external load was calculated by integrating the axial loads recorded atop the piles. To this aim, the distribution of axial load at any instant time was supposed to be symmetrical about the dashed line shown in the plan view of Fig. 4. Fig. 7 illustrates the load-rotation response obtained for the two models belonging to set B. In this case, a direct measurement of the external load was available as the load actuator was equipped with a load cell. For each foundation model, the curve determined by integrating the axial loads carried out by the piles is also plotted for comparison. The two plots are in a very satisfactory agreement for both B1 and B2, giving confidence that the assumption of the symmetry shown in Fig. 4 is appropriate. Notably, the moment-rotation response of group B1 is characterized by two local minima, corresponding to points (b) and (d) in Fig. 7a. The first reduction of load, between points (a) and (b) is due to a temporary reduction of the rate of displacement of the actuator which increased again after point (b), whereas the sudden drop between points (c) and (d) corresponds to a stage in which the actuator stopped due to a malfunction. After this intermediate pause, the displacement rate was set again at 1 mm/s and the load recorded by the actuator started to increase again, between points (d) and (e). The difference between the two plots at very large rotations, between points (e) and (f), is due to the load cell on the actuator coming in contact with the cantilever beam used to apply the eccentric load. This is the same drawback for which the plots related to B2 deviate from each other after local minimum corresponding to point (b), as shown in Fig. 7b.

From a methodological point of view, collapse is identified with the first peak of the load history for all the model foundations. It will be seen that such a definition corresponds also to the occurrence of a kinematical failure. The ultimate axial-moment coordinates (Q_u, M_u) are calculated through the following equations:

$$Q_u = Q_{\max}[Q_{\min}] + W_{pile} + W_{cap} \tag{4a}$$

$$M_u = M_0 - Q_{\max}[Q_{\min}] \cdot e = W_{beam} \cdot e_0 - Q_{\max}[Q_{\min}] \cdot e \tag{4b}$$

where M_0 is the initial moment due to the cantilever beam, e_0 the lever arm of the weight W_{beam} of the cantilever beam, W_{pile} the weight of the piles, W_{cap} the weight of the cap and the cantilever beam, e the eccentricity of the external load, $Q_{\max}$ the first local maximum of the external load for model foundations A1, A2 and B1, while $Q_{\min}$ is the first local minimum of the external load for model B2. The above ultimate coordinates are summarised in Table 3, from which it is easy to build up the load paths followed in the centrifuge.

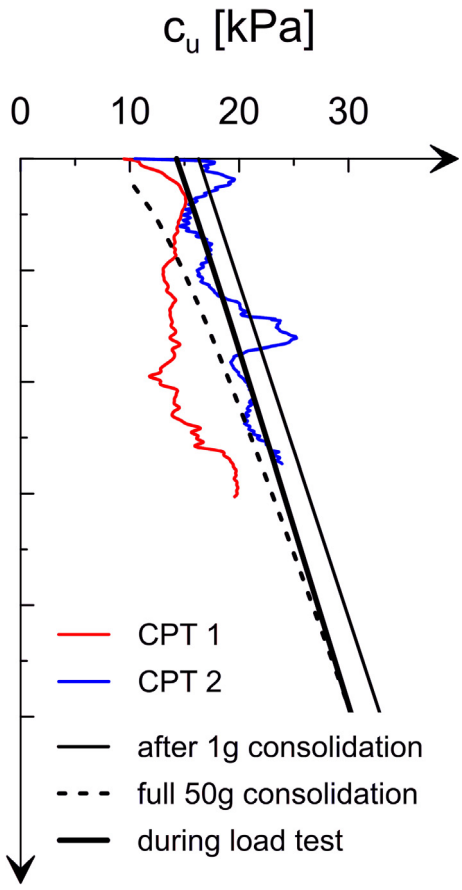

Fig. 5. Profile of theoretical and experimental undrained shear strength profiles (modified after de Sanctis et al. 2021).

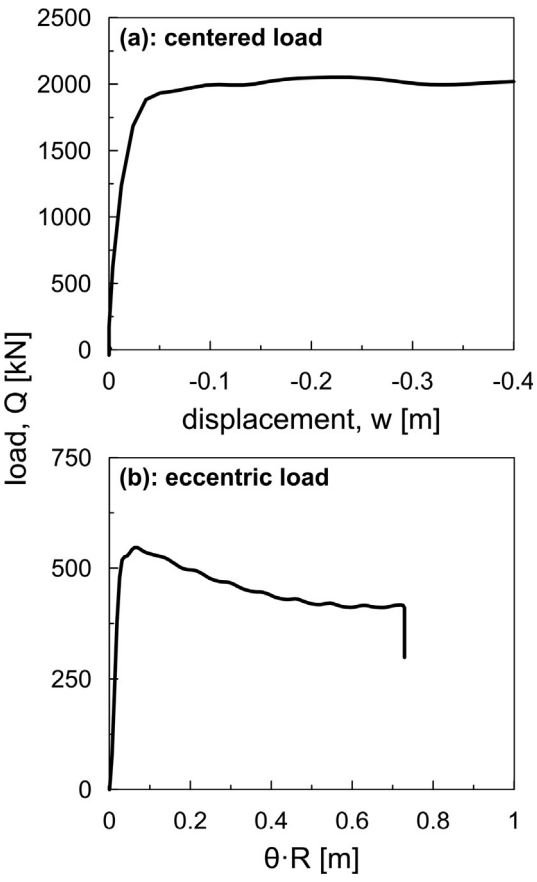

Fig. 6. (a) Load-settlement curve of pile group A1, and (b) load-rotation curve of pile group A2.

4. Experimental validation of the equations for interaction diagrams

It is useful to first analyse in more detail the load distribution on piles at failure. Fig. 8 shows this axial load distribution for set A. For test A1, the load distribution is quite uniform, with a mean value of 408 kN. The efficiency factor (Kezdi 1957), defined as the pile group capacity divided by the axial capacity of the isolated piles multiplied by the number of piles, is equal to 0.9, in line with literature indications (e.g. Fleming et al 2008). For pile group A2, the distribution of loads at collapse involves both compressive and tensile axial forces. Particularly, piles 5, 4–6 and 3–7 reach a load value which is very similar to the capacity determined experimentally for the isolated pile. The same holds for the tensile load on pile 1. Piles 2–8, instead, attain a tension load which is far smaller than their uplift capacity.

Table 2
Axial capacity in compression, N_u, and in uplift, ($-S_u$) of isolated piles.

Test	Series	$Q_{max}[Q_{min}]$ (kN)	$N_u[-S_u]$ (kN)	W (kN)
Uplift	A	−379	−267	112
Compression	A	341	455	114
Uplift	B	–323	−204	119
Compression	B	381	496	115

Fig. 9 reports the results for set B. In B1, axial loads on piles 5, 4–6 and 3–7 are higher than the capacity in compression of the isolated pile, while pile 1 attains a load which is lower than the uplift capacity ($-S_u$). Piles 2–8 are subjected to a compressive load which is lower than N_u. In summary, for low-eccentricity test B1, the piles' capacities in the group deviate to some extent from the ones observed for the isolated piles. Such behaviour is attributed mainly to the variability in the shaft capacity, which is very sensitive to the unavoidable random irregularities in the sand film around piles. The scattering field between loads recorded on instrumented piles and the capacity determined from isolated piles is even more pronounced in test B2. At collapse, the tensile load on piles 5, 4–6 and 3–7 ranges between −107 and −307 kN, while the uplift capacity of the isolated pile is −204 kN. Conversely, the compressive load on pile 1, equal to 412 kN, is quite close to N_u. A noteworthy point is that the pile base resistance is in principle not affected by the irregularities of the sand film around the pile, and this explains why tension loads at failure on piles belonging to group B2 are more erratic then compression loads on piles belonging to B1.

Fig. 10 reports the load paths of tests A1 and A2 as compared to the interaction domains constructed from

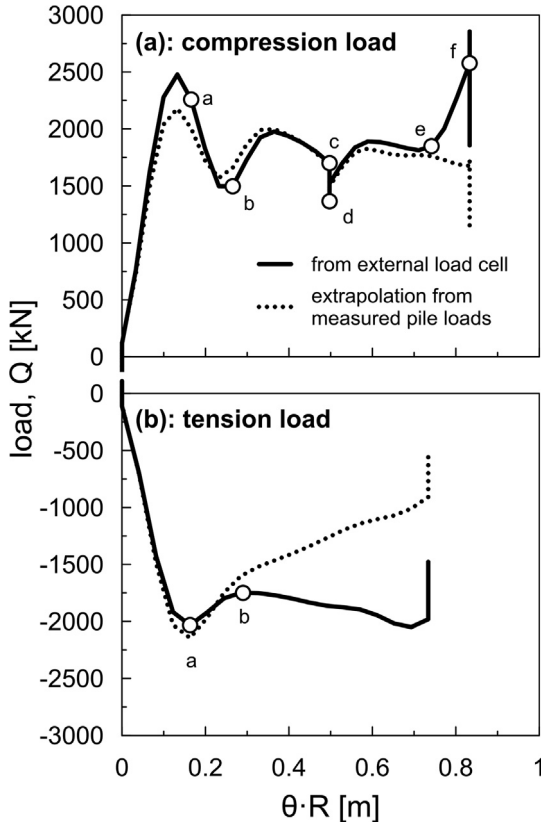

Fig. 7. Load-rotation curves of (a) pile group B1, and (b) pile group B2.

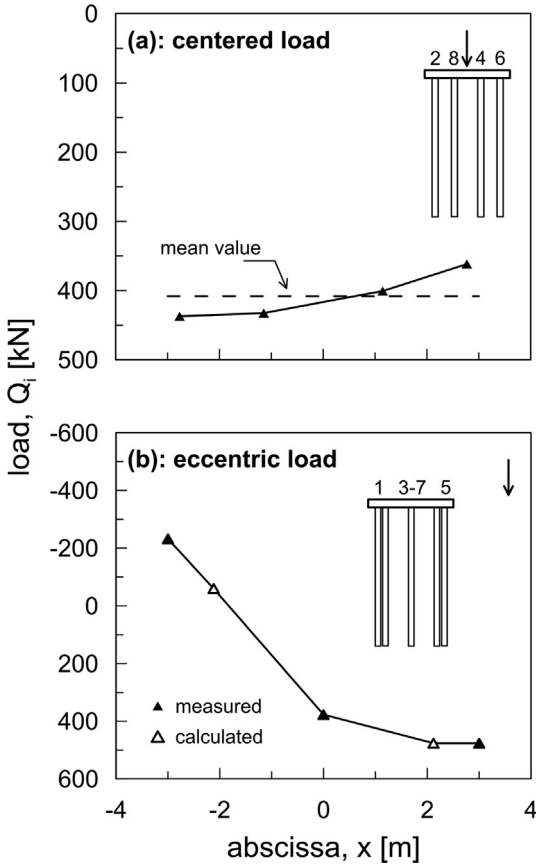

Fig. 8. Distribution of axial load on piles at failure for (a) pile group A1, and (b) pile group A2.

the values of N_u and S_u determined after the single pile tests. Since the pile groups under investigation may be considered as a row of 5 piles, where the central piles have double capacity as compared to the end piles, the innovative domain is made up of 10 vertices. Load paths consist of 3 points connected by 2 lines. The first point represents only the weight of piles W_{piles}, the second point includes the weight of the cap and the beam W_{cap} and, if any, the initial moment M_0 while the last point is representative of the ultimate values of axial force and moment. For pile group A2, the slope of the first line is the lever arm of W_{beam}, while the slope of the second line is the eccentricity e of the applied vertical load. While load path A1, made up of two horizontal lines, stops at about 90% of the pile group capacity calculated from N_u, the endpoint of A2 falls far beyond the conventional domain to lie on the innovative failure locus.

Fig. 11 shows the outcome of tests B1 and B2. The load paths stop beyond the calculated failure domains, especially for test in compression. This is due to the piles belonging to the group behaving differently from the isolated ones. To gain further insight, the interaction domains may be determined considering the piles as dissimilar, and thereby 16 values of failure loads are needed, 8 in compression and 8 in uplift. Four values are recorded, two values may be obtained by imposing the symmetry condition about the plane of the applied moment, while for the remaining 10 values the capacities of the single pile in compression and uplift may be considered. This leads to the failure envelopes plotted in in Fig. 12. Notably, the conventional domain is no longer a rhombus nor a rhomboid. For both the model foundations, the endpoint of the load path outstrips the conventional domain and falls in close proximity of the innovative failure locus.

The above results show that the capacity of a pile group under eccentric load is much larger than the one obtained

Table 3
Axial-moment capacities of the model foundations.

Pile group	e (m)	W_{piles} (kN)	W_{cap} (kN)	M_0 (kNm)	$Q_{max[min]}$ (kN)	Q_u (kN)	M_u (kNm)
A1	0	834	379	0	2051	3264	0
A2	7.25	815	481	−440	547	1843	−4402
B1	1.45	822	424	−14	2478	3724	−3608
B2	1.45	840	433	−17	−2033	−759	2930

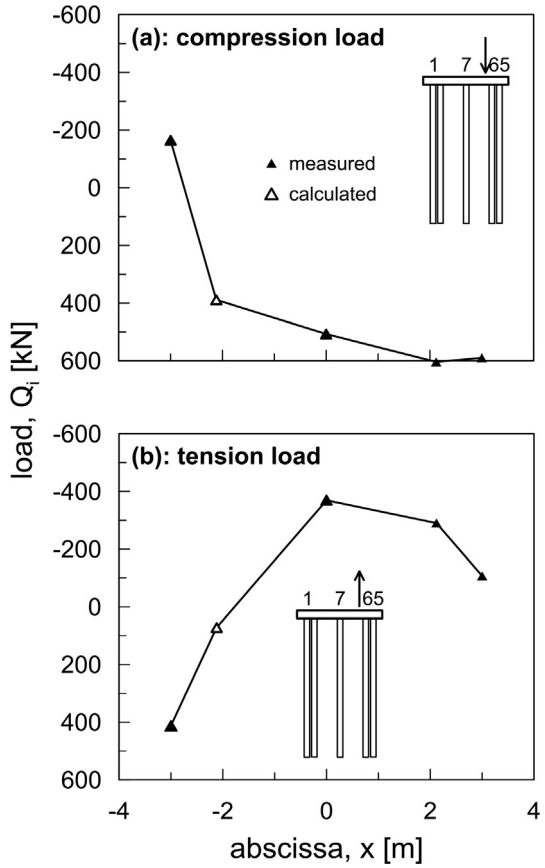

Fig. 9. Distribution of axial load on piles at failure for (a) pile group B1, and (b) pile group B2.

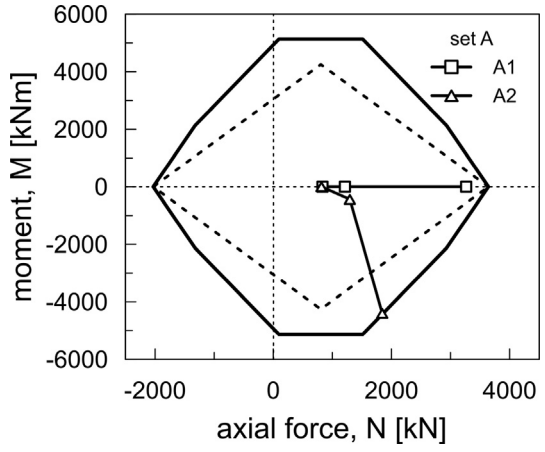

Fig. 10. Conventional (dashed line) and innovative (continuous line) domain for pile groups A1 and A2.

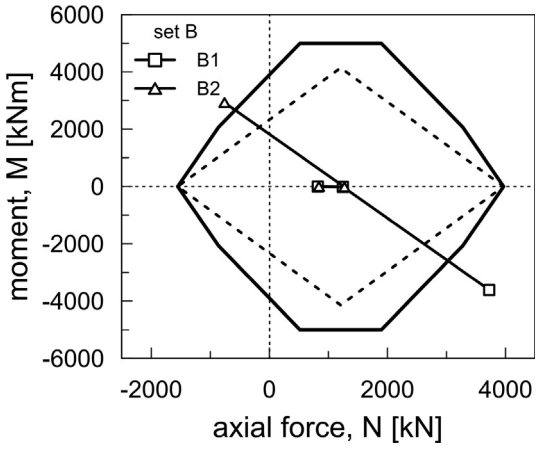

Fig. 11. Conventional (dashed line) and innovative (continuous line) domain for pile groups B1 and B2 under the assumption of identical piles.

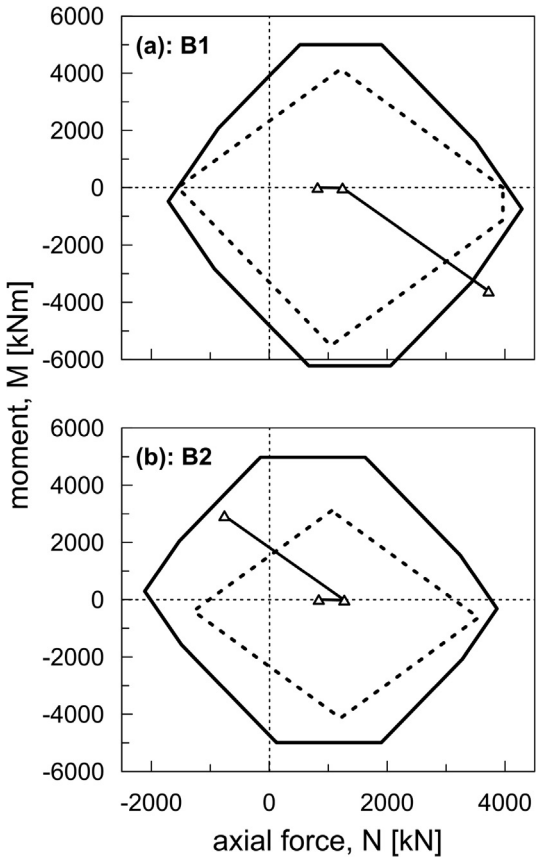

Fig. 12. Conventional (dashed line) and innovative (continuous line) domain under the assumption of dissimilar piles for (a) pile groups B1, and (b) pile group B2.

considering the mobilization of the axial capacity on the outermost pile as the failure of the pile group. Particularly, the distance between the endpoint of load path B2 from the inner domain is paradigmatic of the inherent amount of conservatism of current industry-based design methods.

In summary, the predictive capability of the interaction diagrams based on the limit analysis has proven to be fully satisfactory.

5. Collapse mechanism of pile groups under axial-moment loading

As a further step, it is interesting to investigate the capability of the innovative approach to predict also the collapse mechanism. In the hypothesis of piles behaving as rigid-plastic elements, the collapse occurs through a rotation about

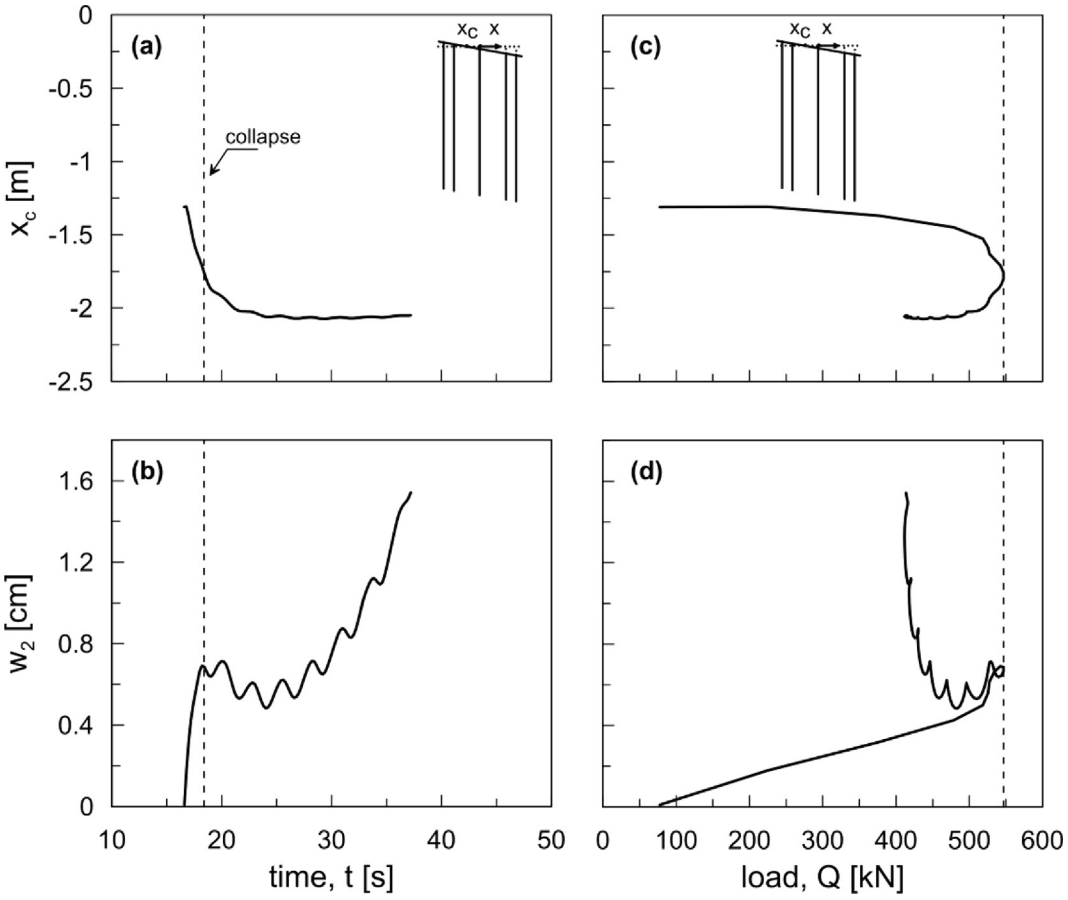

Fig. 13. Variation of the abscissa of the centre of rotation and the displacement of pile No. 2 with time (a, b) and external load (c, d).

a pile or a piles' alignment, and the rotational collapse mechanism about each alignment is associated to a specific segment of the domain. From the experimental campaign under consideration it is possible to investigate the displacement pattern before and after collapse. In this work, we focus for brevity on test A2, corresponding to a vertical load with high eccentricity. Fig. 13(a,b) depicts the time-varying abscissa of the centre of rotation (i.e. the point having zero vertical displacement), x_c, and the vertical displacement of the alignment 2–8, w_2, which is the one around which the group rotates at collapse according to the theory. The same quantities are also reported as function of the applied external load in Fig. 13(c,d). Before collapse, as the load and the rotation increase, the null point moves towards the theoretical position. This is reflected in a less-than-linear increase of w_2. When the group capacity is reached, the null point is very close to the alignment 2–8. From now on, the pile group starts to rotate about the theoretical null point (piles' alignment 2–8), as evident observing that despite rotation is continuously increasing, w_2 remains almost constant until the system undergoes very large displacements.

6. Discussion and conclusion

Piled foundations provide an economical foundation option under circumstances where the performance of the shallow foundation does not meet the design requirements. Under combined axial-moment loading, the most widespread approach is that of identifying the Ultimate Limit State of the pile group with the mobilization of the axial capacity in tension or compression on the outermost pile. This approach, however, is unduly conservative, as it neglects the reserve of capacity that the pile group may provide due to the ductility of pile-soil elements that progressively achieve their axial capacity during the loading process. The focus is set on the solution for failure envelopes of pile groups by Di Laora et al. (2019) based on theorems of Limit Analysis, in which the additional contribution coming from the piles' ductility is implicitly taken into account. Failure envelops are polygons whose number of sides is twice the number of piles and there is a correspondence between each side and the kinematics of failure. While there is theoretical evidence of the advantage that such an approach may provide, the predictive ability of the equations of the above failure envelopes has not yet experimentally validated experimentally. A centrifuge testing program at the Schofield Centre of University of Cambridge has been carried out to this aim. It consisted of two series of centrifuge experiments (A and B) on reduced scale models of pile groups using monotonic load paths under constant eccentricity or constant axial loads. Each series included also two tests on isolated piles,

one in compression and one in uplift. The load tests on isolated pile allowed to build up the analytical interaction domain based on either the conventional or the innovative design approach. For all the examined foundations, the endpoints of the load paths followed in the centrifuge outstrip the conventional failure envelope. While for series A they lie approximately on the failure envelopes proposed by Di Laora et al. (2019), for series B they lie well outside also from this boundary. This result is due to the variability of the behaviour of piles belonging to the group. If this variability is explicitly taken into account, the endpoints of the load paths lie approximately on the outer boundary. Overall, the two series of experiments have proven the validity of the exact solution based on theorems of limit analysis. For pile group under tension load (B2), the distance between the endpoint of the load path and the inner domain is paradigmatic of the excessive conservatism of the conventional approach.

The testing program, from the preparation of the kaolin clay to the application of the external load under constant rate displacement, is fully repeatable. Piles were connected to the raft by hinges and, hence, the external load could not be but equilibrated by axial loads on piles. This allowed an easy interpretation of the pile group behaviour and, also, a swift identification of the collapse load. The main uncertainties of this testing program are related to the variability of the shaft capacity due to the irregularities of the sand film glued on the piles. A detailed inspection of the axial load distribution at failure is mandatory for assessing the scattered field of axial capacities and, eventually, correct the failure envelopes evaluated from loading tests on isolated piles. Notably, not only the equations of the failure locus was validated, but also the intertwined relation between the sides of the polygon and the kinematics of the collapse mechanism. Pile groups indeed fail by rotating about the piles' alignment corresponding to the side of the locus intercepted by the load pattern. Just as the group rotates about piles' alignment 2–8 in test A2, so might we expect it to rotate about 3–7 for a virtual pattern lying on the plateau of the failure locus. It is therefore believed that the proposed approach has general applicability. It must be emphasized that all the above concepts apply only to failure modes involving individual pile capacities (Fleming et al. 2008). However, a pile group may collapse also by failure of the block of soil containing the piles, at least under centred load. This is a far remote mechanism in coarse grained soil. But care must be taken for groups of piles in clay at spacing ratios smaller than some critical value, say 2–4 (Cooke 1986), for which the likelihood of the block failure mechanism must be taken in due consideration.

The very satisfactory agreement between the theoretical framework and the tests carried out with the Turner Beam Centrifuge at the University of Cambridge makes the equations of the new failure envelopes a very promising tool for design of piled foundation under moderate to eccentric vertical load. However, it is fair to mention that the suitability of the design solution obtained by using such an approach must be also checked against serviceability criteria.

Declaration of Competing Interest

The authors declare that they have no known competing financial interests or personal relationships that could have appeared to influence the work reported in this paper.

Acknowledgments

This work has been carried out under a research agreement between University of Napoli Parthenope and the Italian multinational for renewable energies corporation Enel Green Power and research project MIUR PRIN 2017 'A new macro-element model for pile groups under monotonic, cyclic and transient loads' granted by the Italian Ministry for Research and University. We are strongly grateful to Prof. Gopal Madabhushi, Prof. Giulia Viggiani and Dr. Thejesh Garala from University of Cambridge for their support to the execution of the centrifuge testing program.

References

AASHTO, 2012. AASHTO guide specifications for LRFD seismic bridge design, 2nd ed. American Association of State Highway and Transportation Officials, Washing-ton, D.C.

Bransby, M.F., Randolph, M.F., 1998. Combined loading of skirted foundations. *Géotechnique* 48 (5), 637–655.

Brinch Hansen, J. (1970). A revised and extended formula for bearing capacity. Bulletin No. 2, Danish Geotechnical Institute, Copenhagen, Denmark.

Cassidy, M.J., Randolph, M.F., Byrne, B.W., 2006. A plasticity model describing caisson behaviour in clay. Appl. Ocean Res. 28 (5), 345–358.

CEN (2003) (pr)EN 1997-1. Eurocode 7: geotechnical de-sign—part I: general rules. European Committee for Standardization Technical Committee 250, Brussels, Belgium.

Comodromos, E.M., Papadopoulou, M.C., 2012. Response evaluation of horizontally loaded pile groups in clayey soils. Géotechnique 62 (4), 329–339.

Cooke, R.W., 1986. Piled raft foundations on stiff clays: a contribution to design philosophy. Géotechnique 36 (2), 169–203.

de Sanctis, L., Di Laora, R., Garala, T.K., Madabhushi, G.S.P., Viggiani, G.M.B., Fargnoli, P., 2021. Centrifuge modelling of the behaviour of pile groups under vertical eccentric load. Soils Found. 61 (2), 465–479.

Di Laora, R., de Sanctis, L., Aversa, S., 2019. Bearing capacity of pile groups under vertical eccentric load. Acta Geotech. 14 (1), 193–205.

FEMA 750, 2009. Recommended seismic provisions for new buildings and other structures. Building Seismic Safety Council, National Institute of Building, Washington, D.C..

Fleming, W.G.K., Weltman, A.J., Randolph, M.F., Elson, W.K., 2008. Piling engineering. CRC Press.

Franza, A., Sheil, B., 2021. Pile groups under vertical and inclined eccentric loads: Elastoplastic modelling for performance based design. Comput. Geotech. 135 104092.

Gottardi, G., Butterfield, R., 1993. On the bearing capacity of surface footings on sand under general planar load. Soils Found. vol. n. 33(3), 68–79.

Gourvenec, S., 2007. Failure envelopes for offshore shallow foundations under general loading. Géotechnique 57 (3), 715–728.

Gourvenec, S.M., Randolph, M.F., 2003. Effect of strength non-homogeneity on the shape of failure envelopes for combined loading of strip and circular foundations on clay. Géotechnique 53 (6), 575–586.
Gourvenec, S., Barnett, S., 2011. Undrained failure envelope for skirted foundations under general loading. Géotechnique 61 (3), 263–270.
Iovino, M., Maiorano, R.M.S., de Sanctis, L., Aversa, A., 2021. Failure envelopes of pile groups under inclined and eccentric load. Géotechnique Letters 11 (3), 1–7. https://doi.org/10.1680/jgele.21.00059.
Kezdi, A., 1957. Bearing capacity of piles and pile groups. Proceedings of the IV ICSMFE 2, 46–51.
Kishida, H., Meyerhof, G.G., 1965. Bearing capacity of pile groups under eccentric loads in sand. Proc. 6th ICSMFE. Montreal 2, 270–274.
Martin, C.M., Houlsby, G.T., 2000. Combined loading of spudcan foundations on clay: laboratory tests. Géotechnique 50 (4), 325–338.
Meyerhof, G.G., 1981. The bearing capacity of rigid piles and pile groups under inclined loads in clay. Can. Geotech. J. 18 (2), 297–300.
Meyerhof, G.G., Ranjan, G., 1973. The bearing capacity of rigid piles under inclined loads in sand. III: Pile Groups. Can. Geotech. J. 10 (3), 428–438.
Meyerhof, G.G., Yalcin, A.S., 1984. Pile capacity for eccentric inclined load in clay. Can. Geotech. J. 21 (3), 389–396.
Meyerhof, G.G., Yalcin, A.S., Mathur, S.K., 1983. Ultimate pile capacity for eccentric inclined load. Journal of Geotechnical Engineering 109 (3), 408–423.
Nova, R., Montrasio, L., 1991. Settlements of shallow foundations on sand. Géotechnique 41 (2), 243–256.
Papadopoulou, M.C., Comodromos, E.M., 2010. On the response prediction of horizontally loaded fixed-head pile groups in sands. Comput. Geotech. 37 (7–8), 930–941.
Roscoe, K.H., Schofield, A.N., Wroth, C.P., 1958. On the yielding of soils. *Géotechnique* 8 (1), 22–52.
Rose, A.V., Taylor, R.N., El Naggar, M.H., 2013. Numerical modelling of perimeter pile groups in clay. Can. Geotech. J. 50 (3), 250–258.
Saffery, M.R., Tate, A.P.K., 1961. Model tests on pile groups in a clay soil with particular reference to the behaviour of the group when it is loaded eccentrically. In *Proceedings of the Fifth Conference on Soil Mechanics and Foundation Engineering*, pp. 129–134.
Sheil, B.B., McCabe, B.A., 2014. A finite element–based approach for predictions of rigid pile group stiffness efficiency in clays. Acta Geotech. 9 (3), 469–484.
Taiebat, H.A., Carter, J.P., 2000. Numerical studies of the bearing capacity of shallow foundations on cohesive soil subjected to combined loading. Géotechnique 50 (4), 409–418.
Vulpe, C., Gourvenec, S., Power, M., 2014. A generalised failure envelope for undrained capacity of circular shallow foundations under general loading. Geotechnique Letters 4, 187–196.